ISIJ International, Vol. 64 (2024), No. 12, pp. 1820–1828
https://doi.org/10.2355/isijinternational.ISIJINT-2024-191

Effect of P Addition on the Corrosion Resistance of Steels before and after Rust Formation

Chihiro HAYAMA,[1,2] Mariko KADOWAKI,[1)*] Yoshiharu MURASE,[1)] Hideki KATAYAMA,[1)] Toru HARA,[1)] Yuka HARA,[1)] Hikari WATANABE,[2)] Isao SHITANDA[2)] and Masayuki ITAGAKI[2)]

1) National Institute for Materials Science, 1-2-1 Sengen, Tsukuba, Ibaraki, 305-0047 Japan.
2) Department of Pure and Applied Chemistry, Faculty of Science and Technology, Tokyo University of Science, 2641 Yamazaki, Noda, Chiba, 278-8510 Japan.

(*Received June 24, 2024; Accepted August 22, 2024; Advance online published September 3, 2024; Published October 15, 2024; Originally published in Tetsu-to-Hagané, Vol. 110, 2024, No. 7, pp. 548–557*)

This study investigates the effect of P addition on the corrosion resistance of steels before and after rust formation. Electrochemical measurements and surface analysis of P-containing steels (Fe-0.5 mass% P, Fe-1.0 mass% P, and Fe-1.5 mass% P) were conducted to analyze the contribution of P to their initial corrosion resistance before rust formation. The results showed that the initial corrosion resistance of the steel worsened with increasing P content. According to the surface analysis conducted by SEM/EDS, more P segregations at the grain boundaries occurred with higher P content. Polarization measurements indicated that these P segregations became initiation sites for localized corrosion, resulting in a decrease in the initial corrosion resistance.

Although the initial corrosion resistance was worse with higher P content, the long-term corrosion resistance showed the inverse trend, improving with increasing P content. Atmospheric exposure tests at Miyakojima and surface analysis of the rust layers showed that P was incorporated into the rust layer, and it promoted the protective ability against corrosion.

KEY WORDS: P-containing steel; segregation; rust; localized corrosion; polarization; atmospheric exposure test.

1. Introduction

P is a representative alloying element in steel,[1,2] and its presence affects the mechanical properties such as fracture toughness[3,4] and weldability.[5,6] In addition to the mechanical properties, P is known to affect the corrosion properties of steels. In particular, P is thought to have significant effects on the properties of rust layer formed when steel is used for long periods of time in atmospheric corrosive environments. For example, it has been reported that for weathering steel containing P, Cr, and Cu, the protective ability of rust layer was enhanced as the contents of these elements increased, resulting in the improvement of corrosion resistance.[7–9] According to the studies conducted by Okada *et al.*[7] and Misawa *et al.*,[8,9] the addition of these elements changes the rust layer to denser, which contributes to the improvement of protective ability. However, the above studies focused on steels containing not only P but also Cr and Cu; the effects of P alone on the rust structure and corrosion resistance of steels are still unclear.

* Corresponding author: E-mail: KADOWAKI.Mariko@nims.go.jp

In addition to the characteristics of rust layer, P may also affect the corrosion behavior of as-polished steel surface without rust in the initial stage of use. P has a proven tendency to segregate at grain boundaries of steels.[10] Many previous studies have reported that such segregation of alloying elements is responsible for the initiation of localized corrosion.[11–13] Manning *et al.* analyzed the corrosion behavior of type 304L duplex stainless steel in acidic solutions and revealed that the segregation of alloying elements at the microstructural interfaces acted as initiation sites for localized corrosion.[13] Küpper *et al.* analyzed the corrosion resistance of Fe–P alloys containing 0.003–2.5 wt% P in hot nitrate solutions and revealed that the corrosion resistance of the alloys decreased owing to the presence of P segregation.[11] However, these studies focused on the corrosion behavior in acidic pH environments, and almost no research has been conducted in Cl-containing near-neutral pH environments, which is similar to atmospheric corrosive environment where actual steels are widely used.

As mentioned above, although P is a representative alloying element in steels, no studies have comprehensively analyzed the effect of P on corrosion resistance in atmospheric

environments from the initial stage of use to the long-term behavior after extended exposure periods. Therefore, the objective of this study was to comprehensively clarify the effect of P on the corrosion behavior of steels from the initial to extended stages of use. Because the addition of a large amount of P degrades mechanical properties, the P content of actual steels is generally low (less than 0.1 mass%).[14,15] On the other hand, in this study, to show the effect of P more distinctly, three types of steels with larger amounts of P were prepared (Fe-0.5 mass% P, Fe-1.0 mass% P, and Fe-1.5 mass% P), and the corrosion behavior was investigated. First, electrochemical measurements and surface analysis of the as-polished surface without rust were performed to access the effect of P on the initial corrosion resistance. Close attention was paid to the relationship between P segregation and localized corrosion initiation behavior. Additionally, a long-term atmospheric exposure test was conducted to analyze the corrosion resistance with the formation of a rust layer over extended periods of long-term use. SEM/EPMA observation of cross-sections of the rust layers was conducted to analyze the effect of P on rust formation.

2. Experimental

2.1. Specimens

Three types of Fe–P alloys with varying P contents (Fe-0.5 mass% P, Fe-1.0 mass% P, and Fe-1.5 mass% P) were used as specimens. The chemical compositions of the specimens are listed in **Table 1**. The specimens were heated at 1 200°C for 1 h, then hot-rolled at 925±25°C and air-cooled. After the heat-treatment, the specimen surfaces intended for use in polarization measurements were mechanically ground using SiC paper up to 1 500 grit and were finished by polishing with a 1 μm diamond paste. The specimens intended for use in microstructural observation and immersion tests underwent Ar ion milling after the diamond paste polishing. The specimens for use in the atmospheric exposure tests were cut to dimensions of 150 mm × 50 mm× 6 mm.

2.2. Surface Observation and Analysis

To investigate the microstructural characteristics and corrosion morphology of the specimens, scanning electron microscopes (SEM) equipped with energy-dispersive X-ray spectroscopy (EDS) systems were used. The composition of non-metallic inclusions, existence of microscopic segregation of P at grain boundaries, and corrosion morphology after polarization and immersion tests were analyzed using Hitachi High-Tech SU5000 and Octane Elite. The accelerating voltage was 15.0 kV. Macroscopic segregation of P was observed using Carl Zeiss AurigaLaser. The accelerating voltage of SEM observation and EDS analysis were 5.0 kV and 15.0 kV, respectively.

Table 1. Chemical compositions of the specimens (mass%).

Specimen	C	Si	Mn	P	S	Cu	Ni
Fe-0.5 mass% P	<0.01	<0.01	0.01	0.50	<0.01	<0.01	<0.01
Fe-1.0 mass% P	<0.01	<0.01	0.03	0.99	<0.01	0.02	<0.01
Fe-1.5 mass% P	<0.01	<0.01	0.05	1.48	<0.01	0.02	<0.01

2.3. Electrolytes

Polarization measurements and immersion tests were performed in boric-borate buffer solution containing 10 mM NaCl (pH 8.0). The buffer solution was prepared by mixing 10 mM NaCl-containing 0.35 M H_3BO_3 and 10 mM NaCl-containing 0.075 M $Na_2B_4O_7$.

2.4. Potentiodynamic Anodic Polarization

Potentiodynamic anodic polarization was conducted in boric-borate buffer solution with 10 mM NaCl (pH 8.0) under naturally aerated conditions at 298 K. The electrode area was 1.5 cm × 1.5 cm. The counter electrode was a Pt plate and the reference electrode was Ag/AgCl (3.33 M KCl). All potentials cited in this paper are expressed in terms of the Ag/AgCl (3.33 M KCl) electrode. An electrochemical measurement system, HZ-7000 (MEIDEN HOKUTO), was used. Before measurements were taken, cathodic treatment (−1.0 V, 10 min) was conducted to remove any surface oxide film from the specimens. A potential scan began at −1.0 V immediately afterwards. The scan rate was 20 mV min^{-1}.

2.5. Potentiostatic Polarization

To investigate the initiation sites of the localized corrosion on the Fe-1.5 mass% P specimen, potentiostatic polarization was conducted at 0.2 V for 80 s in a boric-borate buffer solution with 10 mM NaCl (pH 8.0), and the surface corrosion morphology was observed by SEM/EDS. The polarization conditions, such as the electrode size, counter electrode, and reference electrode, were the same as those used for the potentiodynamic polarization, as explained earlier.

2.6. Immersion Test

To analyze the effect of P on the initiation of localized corrosion, immersion tests of the Fe-0.5 mass% P, Fe-1.0 mass% P, and Fe-1.5 mass% P specimens were conducted in a boric-borate buffer solution with 10 mM NaCl (pH 8.0). Rectangular regions of 200 μm×300 μm were selected as observation areas, and the number of localized corrosion sites was counted by comparing the optical microscopy images before and after immersion for 3 h.

2.7. Atmospheric Exposure Test

To investigate the effect of P content on long-term corrosion resistance, atmospheric exposure tests of the Fe-0.5 mass% P, Fe-1.0 mass% P, and Fe-1.5 mass% P specimens were conducted at Japan Weathering Test Center, Miyakojima (24°−44'N, 125°−19'E) for a period of 5 years.[16] The specimens, 150 mm × 50 mm× 6 mm in size, were placed facing south at a 45° angle and directly exposed to the atmospheric environment. After 5 years, the weight loss due to corrosion was measured.

2.8. EPMA after Atmospheric Exposure Test

After the atmospheric exposure tests, cross-sections of the specimens were observed using an electron probe micro analyzer (EPMA, JEOL JXA-8500F). To reduce charging effects, a thin conductive coating of Au was deposited on the specimens before observation. The accelerating voltage and probe current for the EPMA were 15.0 kV and 100 nA,

respectively.

3. Results and Discussion

3.1. Microstructure Characterization

To confirm the presence of P in the microstructure, SEM observation and EDS analysis were performed on the surfaces of the specimens after ion-milling. **Figure 1** shows SEM images of the Fe-0.5 mass%, Fe-1.0 mass%, and Fe-1.5 mass% P specimens. For all specimens, grain size was approximately 100 μm. **Figure 2** shows the EDS maps of P for the same areas as those shown in Fig. 1. For the Fe-0.5 mass% P specimen shown in Fig. 2(a), no P distribution/concentration can be observed along the microstructure. On the other hand, for the Fe-1.0 mass% P and 1.5 mass% P specimens shown in Figs. 2(b) and 2(c), band-like high P-concentration areas (macroscopic segregation) were observed in the horizontal direction, indicated in the figures by arrows. Such macroscopic segregation of P is considered to occur during the steel solidification process.[17)]

In addition to the macroscopic segregation mentioned above, P can microscopically exist as the segregation along grain boundaries.[10)] To confirm the existence of grain boundary segregation, further SEM/EDS observations were conducted at a higher magnification than those shown in Fig. 2, and the results are shown in **Fig. 3**. In Figs. 3(a), 3(c), and 3(e), the regions including the grain boundaries were selected for observation. In Figs. 3(b) and 3(d), there is no grain boundary segregation of P on the Fe-0.5 mass% P and Fe-1.0 mass% P specimens. On the other hand, as indicated by the arrow in Fig. 3(f), P segregation along the grain boundary was observed for the Fe-1.5 mass% P specimen. These results indicate that the segregation of P along the grain boundary increased with increasing P content in the steels, and are in agreement with results reported by Suto and Takezawa[18)] and Abe *et al.*[19)] Hereafter, the band-like P segregation observed in the macroscopic regions in Figs. 2(b) and 2(c) is referred to as "macroscopic segregation", and the segregation along the grain boundary in Fig. 3(f) is referred to as "microscopic segregation". In addition to macro- and microscopic segregation, P can also exist as P compounds in steel. However, no P compounds were detected in the specimens used in this study.

3.2. Non-metallic Inclusion

The chemical compositions and morphologies of the non-metallic inclusions were examined using SEM/EDS. For all specimens, the non-metallic inclusions were approximately 2–4 μm in size. **Figures 4** to **6** show the SEM images and EDS maps of the inclusions observed on the Fe-0.5 mass% P, Fe-1.0 mass% P, and Fe-1.5 mass% P specimens, respectively. According to the EDS maps, O, Mn, and Si were detected in the inclusions of all the specimens. These inclusions appeared to be complex oxides of Mn and Si. Size, number, and morphology of the inclusions were highly similar across all specimens. P was not detected in the inclu-

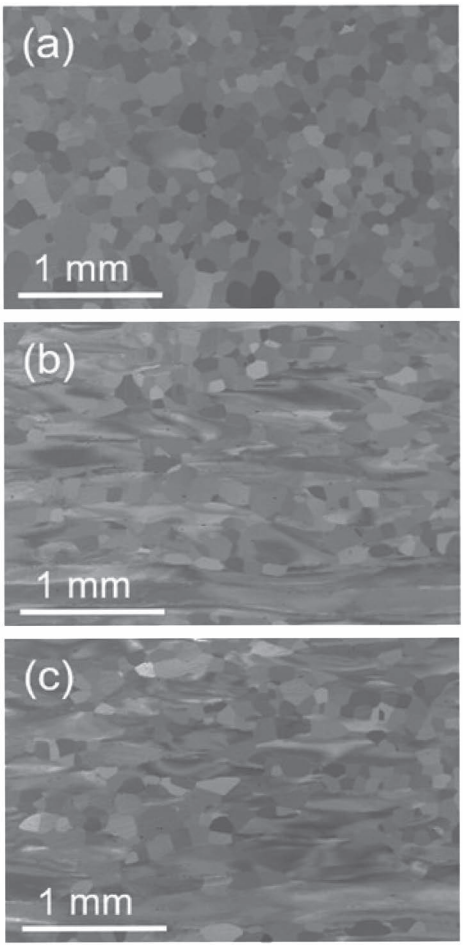

Fig. 1. SEM images of (a) Fe-0.5 mass% P, (b) Fe-1.0 mass% P, and (c) Fe-1.5 mass% P.

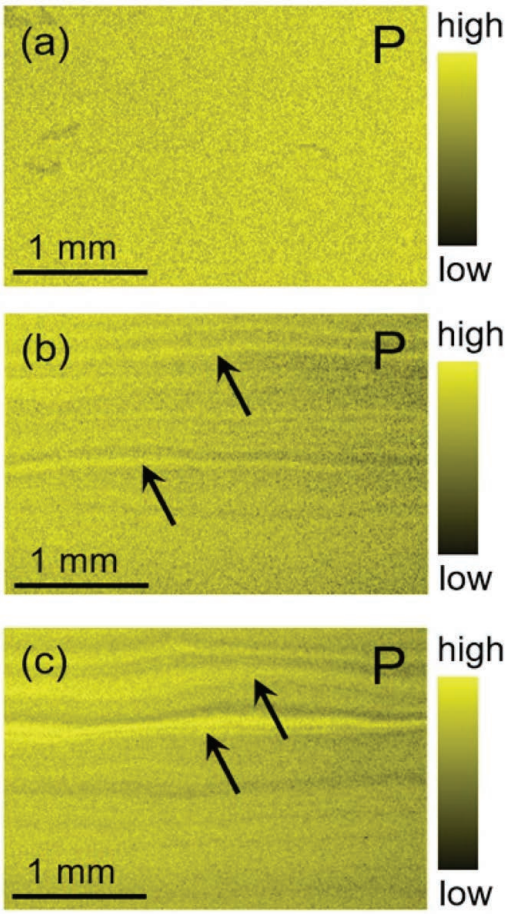

Fig. 2. EDS maps of P on (a) Fe-0.5 mass% P, (b) Fe-1.0 mass% P, and (c) Fe-1.5 mass% P. The same areas were observed as Fig. 1. (Online version in color.)

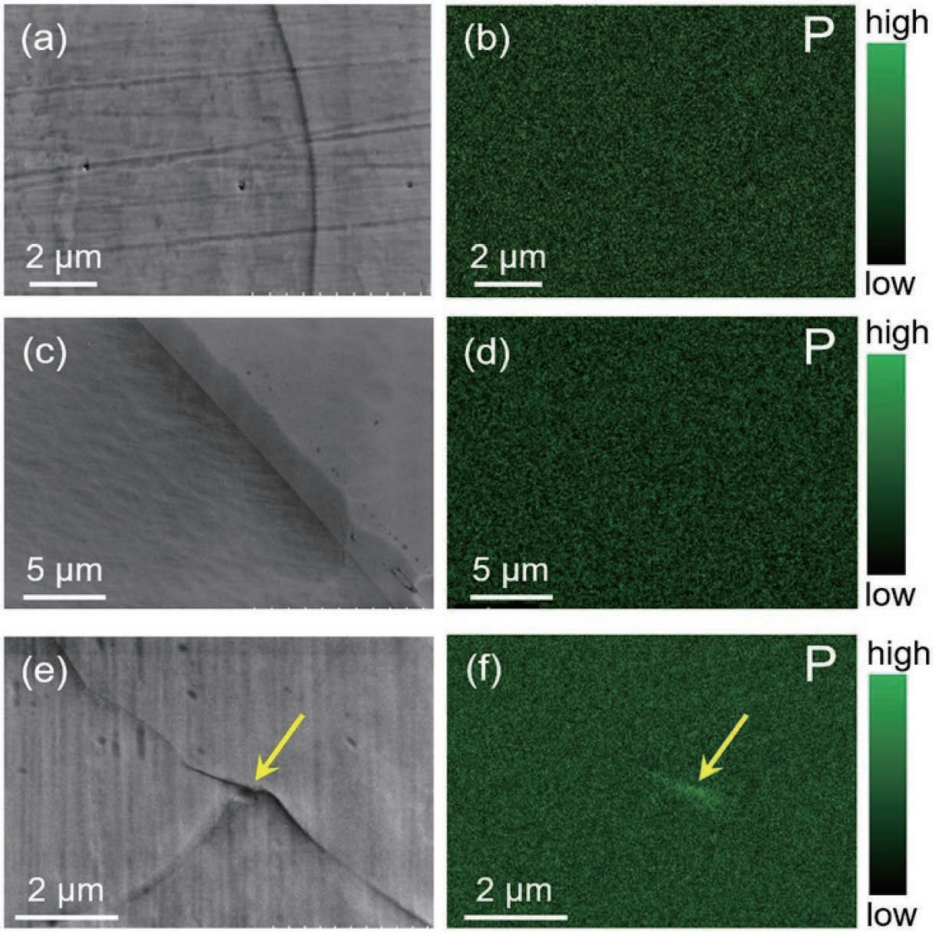

Fig. 3. (a, c, e) SEM images and (b, d, f) EDS maps of P at higher magnification on (a, b) Fe-0.5 mass% P, (c, d) Fe-1.0 mass% P, and (e, f) Fe-1.5 mass% P.

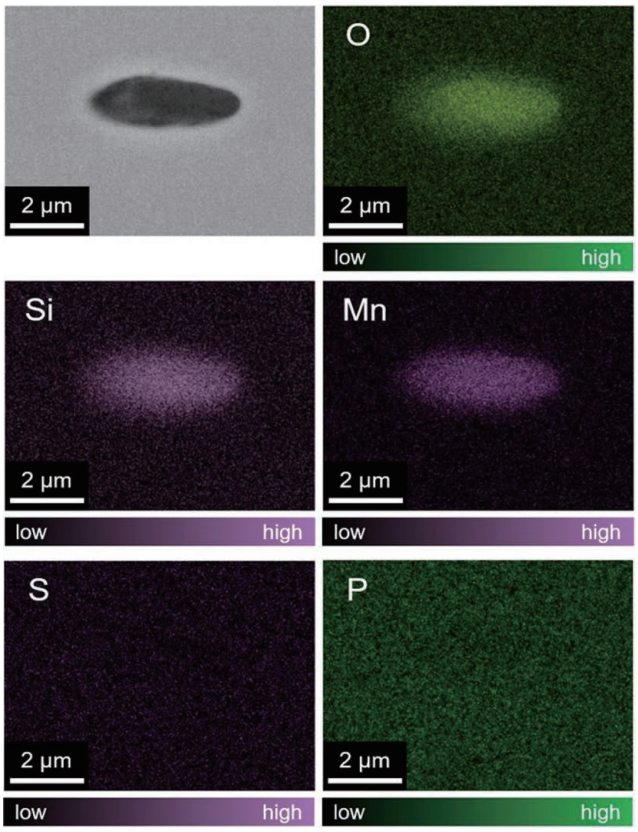

Fig. 4. SEM image and EDS maps of the inclusion on Fe-0.5 mass% P.

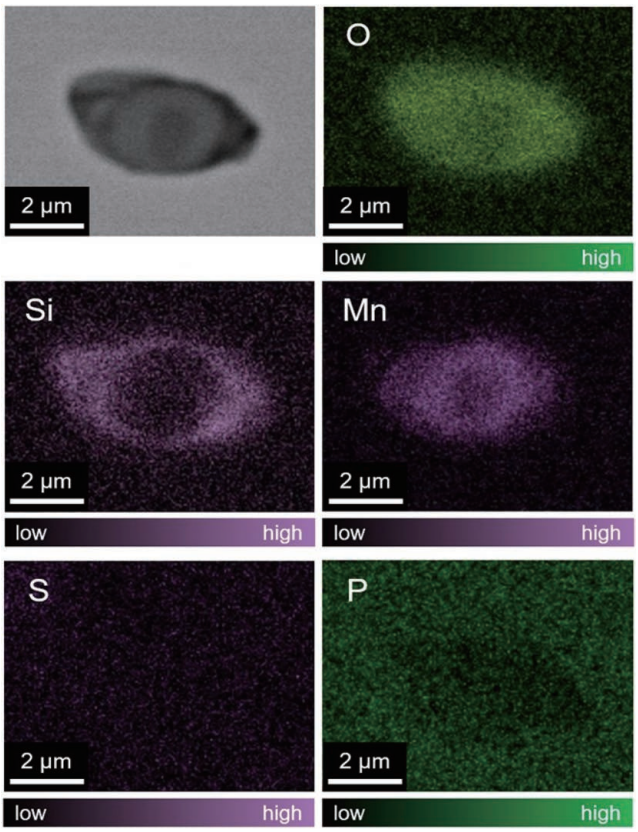

Fig. 5. SEM image and EDS maps of the inclusion on Fe-1.0 mass% P.

sions, as can be seen from the EDS maps.

To summarize the above results, the specimens included two types of P segregation: band-like macroscopic P segregation which was observed on the Fe-1.0 mass% P and Fe-1.5 mass% P specimens, and microscopic P segregation which was observed along the grain boundaries of the Fe-1.5 mass% P specimen only. No P precipitate was observed for any of the specimens, and there was a negligible difference between the characteristics of the non-metallic inclusions. Therefore, by comparing the corrosion behavior of the specimens, the effects of macro- and microscopic P segregation on corrosion resistance can be analyzed.

3.3. Potentiodynamic Anodic Polarization Behavior

To compare the corrosion behavior of the three specimens in NaCl-containing near-neutral pH environments, potentiodynamic anodic polarization was conducted. **Figure 7** shows the polarization curves in a 10 mM NaCl-containing boric-borate buffer solution at pH 8.0. For all specimens, cathodic current was initially measured from −1.0 to −0.65 V, and a subsequent increase in the anodic current due to active dissolution was observed from −0.65 to −0.5 V. Thereafter, cathodic current was temporarily observed from approximately −0.4 to −0.25 V, and then only anodic current was measured in the potential range above −0.25 V. From −0.25 to −0.05 V, anodic current was almost constant and no large increase was detected, suggesting that the specimen surfaces were well passivated at this potential region. There was almost no difference between the polarization curves of all the specimens from the start of polarization to 0.05 V.

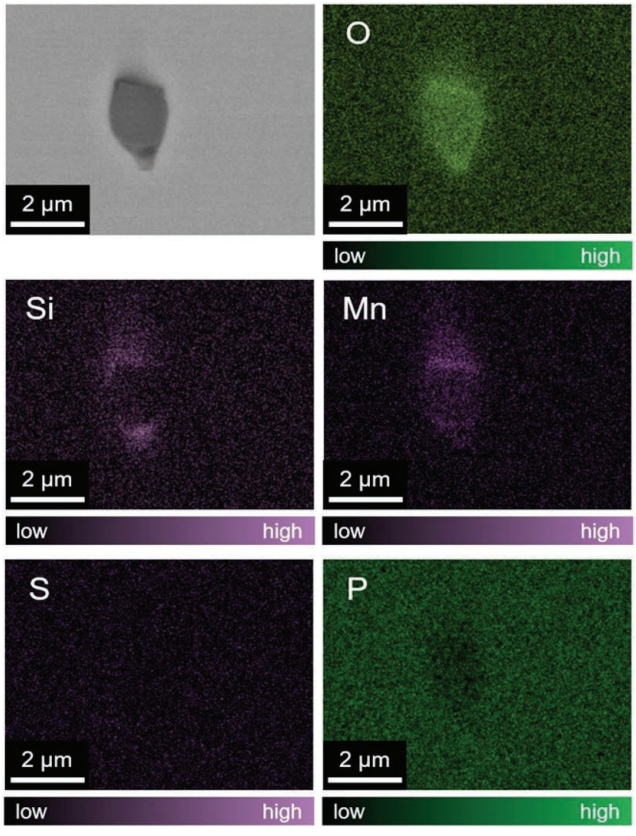

Fig. 6. SEM image and EDS maps of the inclusion on Fe-1.5 mass% P. (Online version in color.)

In the potential range above 0.05 V, a large increase in the anodic current due to the initiation of localized corrosion was observed. For the Fe-1.5 mass% P specimen, which had the highest P content, an increase in the anodic current was observed at a lower potential than those of the other specimens. This indicates that the localized corrosion resistance of the Fe-1.5 mass% P specimen was lower than those of the other specimens. On the other hand, there was almost no difference in the localized corrosion initiation potential between the Fe-0.5 mass% P and Fe-1.0 mass% P specimens.

3.4. Initiation Sites of Localized Corrosion

As shown in Fig. 7, the corrosion resistance of the Fe-1.5 mass% P specimen was lower than those of the other specimens. To clarify the initiation site of localized corrosion on the Fe-1.5 mass% P specimen, potentiostatic polarization was conducted. The specimen was polarized to 0.2 V, which was higher than the initiation potential of localized corrosion in the potentiodynamic polarization curve shown in Fig. 7. **Figure 8** shows the change in the anodic current density with time during potentiostatic polarization. Approximately 10 s after the start of the measurement, a large increase in the anodic current owing to corrosion initiation was observed. Then, 72 s after the increase in the anodic current, polarization was stopped immediately, and the surface corrosion morphology was observed using SEM/EDS.

Figures 9 and **10** show the observation results for the corroded regions. As shown in Fig. 9, after the potentiostatic

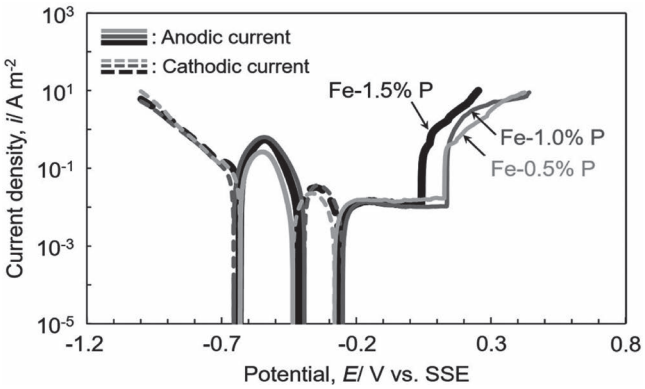

Fig. 7. Potentiodynamic anodic polarization curves in 10 mM NaCl-containing boric-borate buffer solution at pH8.0.

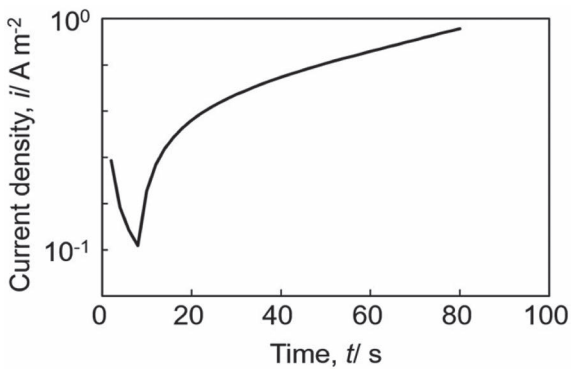

Fig. 8. Change in the anodic current density with time during the potentiostatic polarization at 0.2 V of Fe-1.5 mass% P in 10 mM NaCl-containing boric-borate buffer solution at pH8.0.

polarization, some localized corroded regions 2–5 μm in size were observed on the specimen surface, as indicated by arrows. The EDS maps revealed high concentrations of both Si and Mn within the corroded regions. Considering that the specimens used in this study contained Mn and Si complex oxide inclusions (see Figs. 4–6), the initiation site of the localized corrosion in Fig. 9 appeared to be such inclusion. It is well known that sulfide inclusions typically act the initiation sites for localized corrosion on steels.[20] In addition to the sulfide inclusions, the results shown in Fig. 9 indicate that Mn and Si complex oxide inclusions can also act as initiation sites for localized corrosion in NaCl-containing near neutral pH environments.

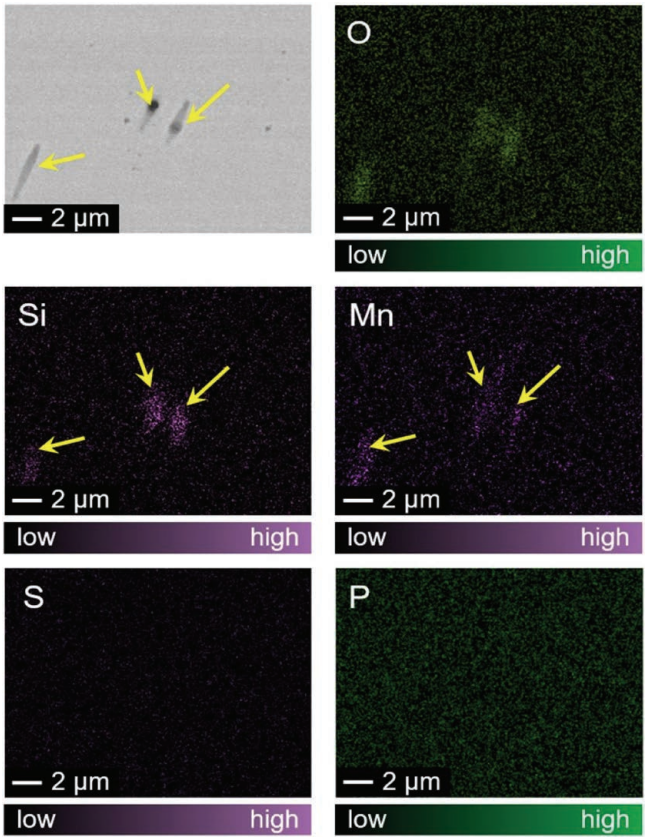

Fig. 9. SEM image and EDS maps of the localized corrosion area with inclusions on Fe-1.5 mass% P after the measurement shown in Fig. 8. (Online version in color.)

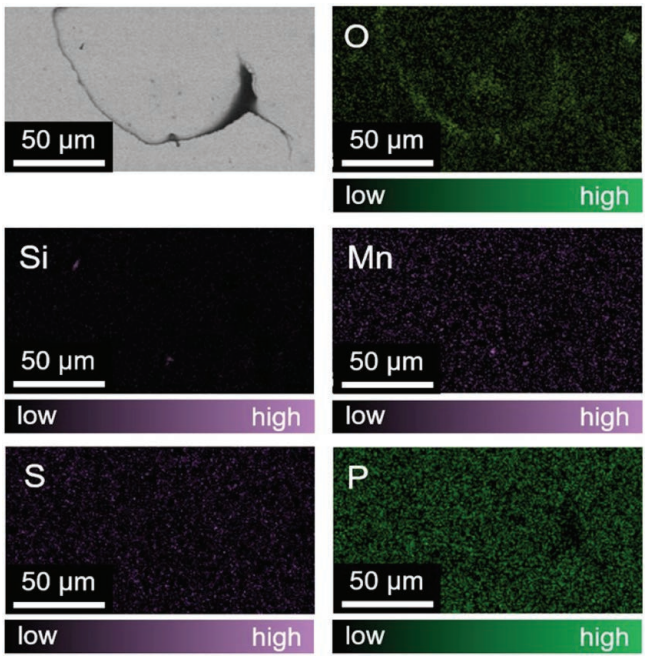

Fig. 10. SEM image and EDS maps of the localized corrosion area without inclusions on Fe-1.5 mass% P after the measurement shown in Fig. 8. (Online version in color.)

In addition to the localized corrosion initiated at the Mn and Si complex oxide inclusions, another type of localized corrosion occurred on the Fe-1.5 mass% P specimen after potentiostatic polarization, as shown in Fig. 10. This localized corrosion region is elongated and narrow. Unlike the corroded areas in Fig. 9, where Mn and Si was detected, the absence of these elements in Fig. 10 suggests that the corrosion initiation site in this case cannot be attributed to Mn and Si complex oxide inclusions. Considering that microscopic P segregation along the grain boundaries existed on the Fe-1.5 mass% P specimen (see Fig. 3), it is estimated that the initiation of localized corrosion in Fig. 10 is likely attributed to such microscopic P segregation.

3.5. Relationship between P Content and Localized Corrosion at Grain Boundary

The results in the previous section indicate that in addition to Mn and Si complex oxide inclusions, microscopic P segregation along grain boundaries appeared to act as the initiation site of localized corrosion. To demonstrate the localized corrosion initiation behavior at P segregation more clearly, immersion tests of the Fe-1.5 mass% P, Fe-1.0 mass% P, and Fe-0.5 mass% P specimens were conducted. For the immersion tests, 200 μm×300 μm regions of the specimens were selected as the observation areas. The specimens were immersed in a 10 mM NaCl-containing boric-borate buffer solution for 3 h, then, the number of localized corrosion sites was counted by comparing the optical microscopy images before and after immersion.

Figures 11(a)–11(c) show optical microscopy images after immersion. For the Fe-0.5 mass% P and Fe-1.0 mass% P specimens shown in Figs. 11(a) and 11(b), respectively, no localized corrosion can be observed along the grain boundaries. By contrast, for the Fe-1.5 mass% P specimen shown in Fig. 11(c), distinct localized corrosion can be

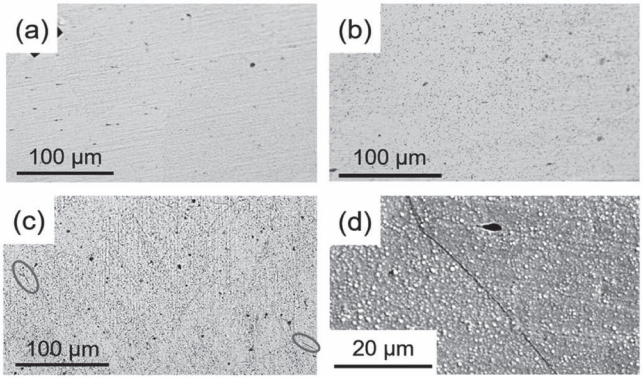

Fig. 11. (a–c) Optical microscope images of (a) Fe-0.5 mass% P, (b) Fe-1.0 mass% P, (c) Fe-1.5 mass% P after the immersion tests in 10 mM NaCl-containing boric-borate buffer solution at pH8.0. (d) is SEM image of intergranular corrosion on Fe-1.5 mass% P.

observed at some grain boundaries. In particular, the deeply corroded grain boundaries are indicated by circles in Fig. 11(c), and the result of the SEM observation of such corroded grain boundary was shown in Fig. 11(d). Localized corrosion proceeded linearly, forming a deeper trench.

Based on the results in Fig. 11, the percentage of grain boundaries that initiated localized corrosion out of all grain boundaries within a 200 μm×300 μm observation area was calculated. For the Fe-0.5 mass% P and Fe-1.0 mass% P specimens, because no localized corrosion existed along the grain boundaries, the percentage was 0%. For the Fe-1.5 mass% P specimen, the percentage of grain boundaries that initiated localized corrosion was 9.5%. This clearly indicates that the corrosion resistance at the grain boundaries of the Fe-1.5 mass% P specimen was lower than that of the other specimens.

For Fig. 3, only the Fe-1.5 mass% P specimen contained microscopic P segregation along grain boundaries, and for the potentiostatic polarization (Figs. 8 and 9) and immersion tests (Figs. 10 and 11), localized corrosion along grain boundaries was initiated on only the Fe-1.5 mass% P specimen. Based on these results, the microscopic P segregation can be concluded to have acted as the initiation sites for localized corrosion along grain boundaries for the Fe-1.5 mass% P specimen, as shown in Figs. 10(c) and 11(c). This decreased the corrosion resistance of the Fe-1.5 mass% P specimen compared to the other specimens, as shown by the potentiodynamic polarization in Fig. 7. Notably, according to the EDS analysis shown in Fig. 10, the localized corrosion region did not contain a higher concentration of P. Therefore, the segregated P appeared to dissolve in solution. In this study, the experiments were conducted in a near-neutral pH solution. In such environments, P dissolves as phosphoric ions (such as HPO_4^{2-} or PO_4^{3-}) via a hydrolysis reaction.[21] The formation of H^+ through this reaction contributes to the local acidification of the surrounding area, which may be a factor that causes localized corrosion initiation at P segregation sites.

3.6. Change in the Initial Corrosion Resistance Depending on P Content

Based on the above results, microscopic P segregation along grain boundaries on the Fe-1.5 mass% P specimen acted as the initiation site of localized corrosion; this appears to be one reason for the lower corrosion resistance. On the other hand, in addition to the microscopic P segregation, the Fe-1.0 mass% P and Fe-1.5 mass% P specimens contained band-like macroscopic segregation (Fig. 2). In previous studies, the macroscopic segregation of alloying elements was reported to act as the initiator for corrosion in acidic pH environments.[12] However, under the experimental conditions of this study, because there was almost no difference between the localized corrosion initiation potentials of the Fe-1.0 mass% P and Fe-0.5 mass% P specimens (Fig. 7), macroscopic P segregation seems to have had little effect on corrosion resistance compared to microscopic segregation. One possible reason between the contributions of macro- and microscopic segregation to localized corrosion is the effect of structural factors at grain boundaries. According to a previous study, some structural features of grain boundaries, such as steps and broken bonds, contribute to an increase in the dissolution rate.[22] As such, the dissolution rate at microscopic segregation was likely higher than that at macroscopic segregation, resulting in the initiation of localized corrosion occurring readily at microscopic segregation.

In summary, the initial corrosion resistance of the as-polished steel surfaces of the specimens decreased with increasing P content. Higher P content increased the existence of microscopic P segregation along the grain boundaries, which appeared to act as initiation sites of localized corrosion.

3.7. Long-term Corrosion Resistance Analyzed by Atmospheric Exposure Test

Thus far, the analysis has focused on examining the corrosion behavior at the as-polished specimen's surfaces in order to evaluate the effect of P content on the initial corrosion resistance. However, in practical application environments, steels are used for long periods (several decades) with rust formation on their surfaces. Therefore, to clarify the effect of P on corrosion behavior during long-term use, atmospheric exposure tests were conducted for a period of 5 years. **Figure 12** shows the weight loss due to corrosion after this 5-year exposure. The same exposure tests were conducted twice for each specimen, and the average weight loss values are shown in Fig. 12. The weight loss of the Fe-1.5 mass% P specimen was the smallest, and the weight loss across all specimens decreased with increasing P content. This suggests that long-term corrosion resistance was improved with increasing P content. In other words, the relationship between the P content and long-term corrosion resistance is the inverse of that between the P content and the initial corrosion resistance of the as-polished specimens, as previously explained.

3.8. Effect of P on the Formation of Rust Layer

As mentioned above, the long-term corrosion resistance showed the inverse trend to the initial corrosion resistance. The most significant difference between the atmospherically exposed and as-polished specimens was the existence of rust layers on the specimen surfaces. To investigate why specimens with a higher P content showed better long-term corrosion resistance, SEM/EPMA observations were conducted on the cross-sections of the rust layers after the atmospheric exposure tests. The results are shown in **Fig. 13**. The Fe-0.5 mass% P and Fe-1.5 mass% P specimens were used. In Figs. 13(a) and 13(e), the bright area at the bottom of this figure is the steel substrate, and the upper dark area with a thickness of 50 μm–150 μm is the rust layer. The upper area of the rust layer is the resin used to fix the specimen. For the Fe-0.5 mass% P specimen in Fig. 13(b), although some

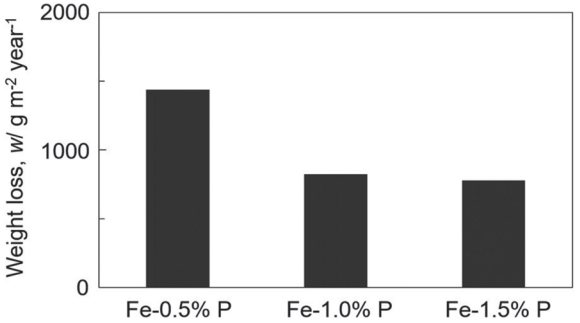

Fig. 12. Weight loss of samples after the atmospheric exposure test at Miyakojima for 5 years.

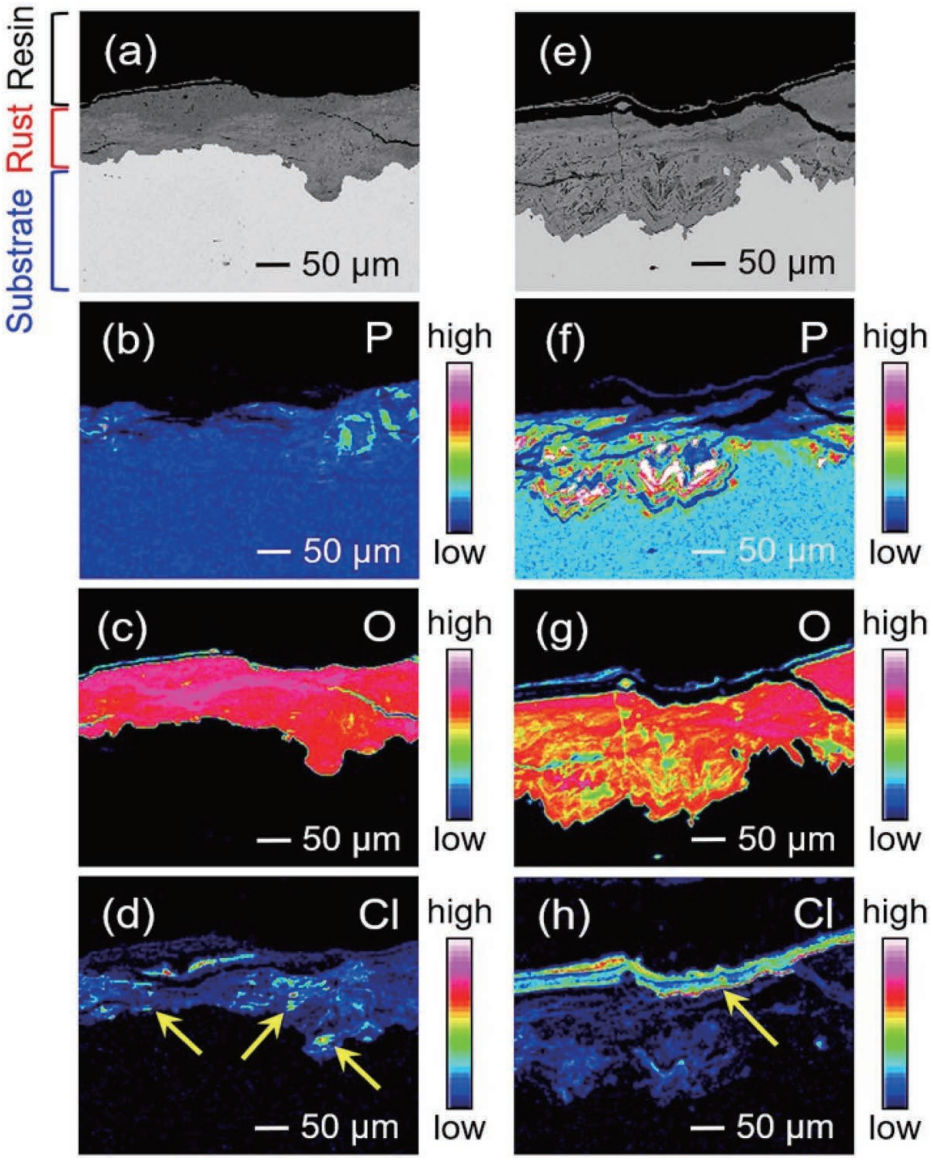

Fig. 13. SEM images and EPMA maps of the cross-sections of (a–d) Fe-0.5 mass% P, (e–h) Fe-1.5 mass% P after the atmospheric exposure test at Miyakojima for 5 years.

P-concentration areas can be observed in the rust layer, P was not enriched in most areas of the rust layer. Additionally, as indicated by the yellow arrow in Fig. 13(d), Cl penetrated the rust layer and reached the steel substrate. This suggests that although a rust layer was formed on the Fe-0.5 mass% P specimen during 5-year exposure, its protective ability was functionally low.

On the other hand, for the Fe-1.5 mass% P specimen, P-enriched areas were observed throughout the rust layer, as shown in Fig. 13(f). In addition, as indicated by the yellow arrow in Fig. 13(h), Cl was detected only at the top of the rust layer, and almost no penetration of Cl into the rust layer was observed. This suggests that the incorporation of P into the rust layer improved the protective ability of the rust layer, resulting in the improvement in the long-term corrosion resistance. It is possible that this improvement of long-term corrosion resistance due to P may be attributed to the change in ion-selective ability. In this study, the experiments were conducted in a near-neutral pH solution. In such environments, P is considered to exist as phosphoric ions in the rust layer.[21,23] According to Miyuki *et al.*, the ion-selective ability of the rust layer is changed by the presence of phosphoric ions, inhibiting the penetration of Cl.[23] In the case of the specimens in this study, the similar change in the ion-selective ability of the rust layer due to phosphoric ions is likely to have contributed to the improvement in the long-term corrosion resistance as shown in Figs. 12 and 13. Further investigation is required to determine the detailed mechanism by which P changes the properties of rust layers.

Based on previous studies, the result that the protective ability of rust layer was improved with increasing P content is reasonable. Okada *et al.* analyzed the relationship between alloying elements and corrosion behavior of weathering steels and reported that the enrichment of P, Cr, and Cu promoted the protective ability of rust layer.[7] Wang *et al.* reported that the incorporation of Cu and P into steel changes the structural characteristics of the rust layer, resulting in the improvement of corrosion resistance.[24] The above studies focused on the properties of the rust layer when several alloying elements such as Cu, Cr, and P were added to the steel together. However, the results of this study suggest that the addition of only a large amount of P

results in a similar change in the structure and composition of the rust layer, which contributes to the improvement in long-term corrosion resistance.

3.9. Comprehensive Effect of P from Initial to Long-term Corrosion Resistance

Based on the above results, the effect of P on the corrosion resistance of steels from the initial to extended stages of use is considered as follows: In the initial stage of use, the corrosion resistance decreases with increasing P content. This is because P segregation along grain boundaries occurs in steel with a high P content, and the segregation sites act as initiation sites for localized corrosion. The segregated P appeared to dissolve in the solution during corrosion. In the later stage of use with rust formation, corrosion resistance is improved with increasing P content, the inverse trend to that for the initial corrosion resistance. This is because P is incorporated into the rust layer, forming a protective layer and thereby enhancing the corrosion resistance.

In this study, to demonstrate the significant effect of P on the corrosion resistance, we used specimens containing larger amounts of P compared to actual steels. On the other hand, it has been reported that the addition of P affected the corrosion resistance of steels even at a P concentration range equivalent to that of actual steels.[11,24,25] Furthermore, although the corrosion behavior of the specimens was investigated in NaCl-containing boric-borate buffer in this study, similar phenomena due to P have been reported in more severe corrosive environments, such as seawater and NaCl solutions.[26–28] Additional research is needed, such as the quantification of P content-dependent change in corrosion resistance, in order to apply these research findings towards enhancing the corrosion resistance of steels employed in practical applications.

4. Conclusions

(1) Based on SEM/EDS observations of three specimens with different P contents, band-like macroscopic P segregation was observed on the Fe-1.0 mass% P and Fe-1.5 mass% P specimens, and microscopic segregation of P along grain boundaries was observed on only the Fe-1.5 mass% P specimen.

(2) Polarization measurements of the as-polished specimens revealed that the initial corrosion resistance of the Fe-1.5 mass% P specimen was lower than those of the other specimens. In addition, after the immersion tests, localized corrosion along grain boundaries was initiated only on the Fe-1.5 mass% P specimen. Considering the microscopic segregation of P along grain boundaries identified for the Fe-1.5 mass% P specimen, such segregation appeared to act as the initiation site for localized corrosion, resulting in decreased corrosion resistance.

(3) Considering the weight loss after the atmospheric exposure tests, the long-term corrosion resistance of the specimens increased with increasing P content, the inverse trend to that of the initial corrosion resistance.

(4) SEM/EPMA observations after atmospheric exposure tests revealed that for steel with a higher P content, P was incorporated into the rust layer, inhibiting the penetration of Cl. In other words, the addition of P improved the protective ability of the rust layer against corrosion.

Statement for Conflict of Interest

The authors declare that they have no known competing financial interests or personal relationships that could have appeared to influence the work reported in this paper.

Acknowledgements

This study was supported by the 32 nd ISIJ Research Promotion Grant (Ishihara/Asada Grant) from the Iron and Steel Institute of Japan. The authors thank Mr. Mitsuaki Nishio for his support in EPMA analysis.

REFERENCES

1) H. Kubo, N. Maruoka and Y. Sato: *Tetsu-to-Hagané*, **105** (2019), 871 (in Japanese). https://doi.org/10.2355/tetsutohagane.TETSU-2019-023
2) M. Sasabe, Y. Iida and T. Yokoo: *Tetsu-to-Hagané*, **100** (2014), 325 (in Japanese). https://doi.org/10.2355/tetsutohagane.100.325
3) K. Abiko: *Materia Jpn.*, **33** (1994), 11 (in Japanese). https://doi.org/10.2320/materia.33.11
4) M. Yamaguchi: *J. Jpn. Inst. Met.*, **72** (2008), 657 (in Japanese). https://doi.org/10.2320/jinstmet.72.657
5) F. Matsuda: *J. Jpn. Weld. Soc.*, **36** (1967), 973 (in Japanese). https://doi.org/10.2207/qjjws1943.36.973
6) K. Hosoi and N. Hara: *J. Jpn. Weld. Soc.*, **78** (2009), 555 (in Japanese). https://doi.org/10.2207/jjws.78.555
7) H. Okada, Y. Hosoi, K. Yukawa and H. Naito: *Tetsu-to-Hagané*, **55** (1969), 355 (in Japanese). https://doi.org/10.2355/tetsutohagane1955.55.5_355
8) T. Misawa, T. Kyuno, W. Suëtaka and S. Shimodaira: *Corros. Sci.*, **11** (1971), 35. https://doi.org/10.1016/S0010-938X(71)80072-0
9) T. Misawa, M. Yamashita and H. Nagano: *Materia Jpn.*, **35** (1996), 783 (in Japanese). https://doi.org/10.2320/materia.35.783
10) M. Kadowaki, I. Muto, H. Katayama, H. Masuda, Y. Sugawara and N. Hara: *Corros. Sci.*, **154** (2019), 159. https://doi.org/10.1016/j.corsci.2019.04.019
11) J. Küpper, H. Erhart and H. J. Grabke: *Corros. Sci.*, **21** (1981), 227. https://doi.org/10.1016/0010-938X(81)90032-9
12) M. Kaneko and S. Abe: *Tetsu-to-Hagané*, **81** (1995), 857 (in Japanese). https://doi.org/10.2355/tetsutohagane1955.81.8_857
13) P. E. Manning, C. E. Lyman and D. J. Duquette: *Corrosion*, **36** (2017), 246. https://doi.org/10.5006/0010-9312-36.5.246
14) M. Morcillo, I. Díaz, B. Chico, H. Cano and D. de la Fuente: *Corros. Sci.*, **83** (2014), 6. https://doi.org/10.1016/j.corsci.2014.03.006
15) T. Kawakubo, T. Nagira, K. Ushioda and H. Fujii: *Tetsu-to-Hagané*, **106** (2020), 892 (in Japanese). https://doi.org/10.2355/tetsutohagane.TETSU-2020-057
16) National Institute for Materials Science: Corrosion Data Sheet, (2016).
17) Y. Nakagawa and A. Momose: *Tetsu-to-Hagané*, **50** (1964), 2175 (in Japanese). https://doi.org/10.2355/tetsutohagane1955.50.13_2175
18) H. Suto and H. Takezawa: *J. Japan Inst. Metals*, **41** (1977), 1166 (in Japanese). https://doi.org/10.2320/jinstmet1952.41.11_1166
19) T. Abe, K. Tsukuda, H. Tagawa and I. Kozasu: *Tetsu-to-Hagané*, **74** (1988), 2201 (in Japanese). https://doi.org/10.2355/tetsutohagane1955.74.11_2201
20) K. Ono and T. Kohno: *Denki Seiko*, **51** (1980), 122.
21) M. Pourbaix: Atlas of Electrochemical Equilibria in Aqueous Solutions, NACE International Cebelcor, Houston, TX, (1974), 504. ISBN978-0915567980
22) Y. Wang, M. Li and H. Ren: *Chem. Mater.*, **35** (2023), 4243. https://doi.org/10.1021/acs.chemmater.3c00220
23) H. Miyuki, M. Yamashita, M. Fujiwara and T. Misawa: *Zairyo-to-Kankyo*, **47** (1998), 186 (in Japanese). https://doi.org/10.3323/jcorr1991.47.186
24) Y. Wang, X. Mu, Z. Chen, Z. Lin, J. Dong, E. F. Daniel, J. Qi and W. Ke: *Corros. Sci.*, **193** (2021), 109912. https://doi.org/10.1016/j.corsci.2021.109912
25) W. Wei and H. J. Grabke: *Corros. Sci.*, **26** (1986), 223. https://doi.org/10.1016/0010-938X(86)90057-0
26) T. Kato, T. Yokosuka and T. Honda: *Zairyo-to-Kankyo*, **48** (1999), 362 (in Japanese). https://doi.org/10.3323/jcorr1991.48.362
27) T. Fukuzumi and T. Misawa: *Tetsu-to-Hagané*, **88** (2002), 73 (in Japanese). https://doi.org/10.2355/tetsutohagane1955.88.2_73
28) T. Fukuzumi and T. Misawa: *Transactions of JSSE*, **50** (2005), 1 (in Japanese). https://doi.org/10.5346/trbane.2005.1